# On the Detection of Faraday Rotation in Linearly Polarized L-Band SAR Backscatter Signatures

Anthony Freeman, *Fellow, IEEE,* and Sasan S. Saatchi, *Member, IEEE*

***Abstract*—The potentially measurable effects of Faraday rotation on linearly polarized backscatter measurements from space are addressed. Single-polarized, dual-polarized, and quad-polarized backscatter measurements subject to Faraday rotation are first modeled. Then, the impacts are assessed using L-band polarimetric synthetic aperture radar (SAR) data. Due to Faraday rotation, the received signal will include other polarization characteristics of the surface, which may be detectable under certain conditions. Model results are used to suggest data characteristics that will reveal the presence of Faraday rotation in a given single-polarized, dual-polarized, or quad-polarized L-band SAR dataset, provided the user can identify scatterers within the scene whose general behavior is known or can compare the data to another, similar dataset with zero Faraday rotation. The data characteristics found to be most sensitive to a small amount of Faraday rotation (i.e., a one-way rotation $< 20°$) are the cross-pol backscatter [$\sigma°(\mathrm{HV})$] and the like-to-cross-pol correlation [e.g., $\rho(\mathrm{HHHV}^*)$]. For a diverse, but representative, set of natural terrain, the level of distortion across a range of backscatter measures is shown to be acceptable (i.e., minimal) for one-way Faraday rotations of less than 5°, and 3° if the radiometric uncertainty in the HV backscatter is specified to be less than 0.5 dB.**

***Index Terms*—Faraday rotation, polarimetry, synthetic aperture radar (SAR).**

## I. Introduction

IT HAS LONG been known that radio waves passing through the ionosphere may be subject to Faraday rotation, in which a linearly polarized wave has its plane of polarization rotated as it propagates through the plasma, e.g., Thompson *et al.* [1]. The magnitude of this effect depends on the radio frequency, the electron density along the path of propagation, the flux density of the earth's magnetic field, and the angle of the wave propagation direction with respect to the direction of the magnetic field vector. After Evans and Hagfors [2], the Faraday rotation angle may be many multiples of $2\pi$ for high frequencies when the electron density is at its peak. The degree of Faraday rotation is proportional to the inverse square of the frequency so that the effects of Faraday rotation can usually be ignored for radio frequencies above 1–2 GHz, but may be significant at lower frequencies, such as P-band ($\sim$400 MHz). Under certain circumstances, e.g., observations made at midday during solar maximum, Faraday rotation may be a significant problem at L-band ($\sim$1.2–1.4 GHz).

Manuscript received January 24, 2003; revised July 27, 2003. This work was supported by the National Aeronautics and Space Administration.

The authors are with the Jet Propulsion Laboratory, California Institute of Technology, Pasadena, CA 91109 USA.

Digital Object Identifier 10.1109/TGRS.2004.830163

The effect of Faraday rotation on measurements of the polarization scattering matrix using monostatic radars was first addressed by Bickel and Bates [3], who formulated the relation between measured and actual scattering matrices and showed that Faraday rotation is a nonreciprocal effect. Gail [5] addressed the effect of Faraday rotation on synthetic aperture radar (SAR) backscatter measurements at scale lengths smaller than the synthetic aperture length, concluding that, for most cases of interest, this could be ignored. This result was confirmed in [6] and [7].

Other ionospheric effects on radio propagation include absorption, which is negligible at ultrahigh frequencies (and above) [8], except under rare conditions in the auroral or polar regions, when it may reach 1 or 2 dB. Refraction should also be negligible, according to [1]. For SAR measurements, the coherence length of the ionosphere may limit the achievable spatial resolution in azimuth, at frequencies less than or equal to 1 GHz according to [9] and [10]. Path length delays may shift the backscatter returns from their "true" positions. In what follows, it shall be assumed that the spatial resolution and sampling have been chosen so that resolution broadening in azimuth and shifts caused by group delay can be ignored. Path length delays may also yield large phase offsets at low frequencies, which may cause problems in comparing phase measurements from successive observations, such as in repeat-pass interferometry. The standard approach to correct such phase problems caused by ionospheric delay is to combine measurements at two widely separated frequencies [1]. In polarimetric measurements, this type of phase error does not usually impact the measurements, since only relative phases between polarizations (which are measured at the same time) are of interest. It is assumed here that the differences between path lengths at horizontal (H) and vertical (V) polarizations can be ignored for nearly simultaneous measurements.

Rignot [11] has addressed the effects of Faraday rotation on L-band H polarization SAR data, particularly in the case of the Japanese Earth Resources Satellite 1 (JERS-1) SAR. In his paper, Rignot suggests that a Faraday rotation of $30 \pm 10°$ provides a reasonable explanation of some anomalous scattering behavior observed in JERS-1 data collected over the Amazon rainforest. He also suggests that Faraday rotations may be as large as $\mathbf{\Omega} = 90°$ during periods of intense solar activity.

Wright *et al.* [12] suggest that Faraday rotation angles for a single path through the ionosphere may be as high as 30° during solar maximum. They also model the effects of Faraday rotation on HH, HV, and VV backscatter (i.e., $\sigma°$), with results indicating that values of $\mathbf{\Omega} > 5°$ are likely to significantly affect the recovery of geophysical parameters from these three measures.

Faraday rotation may be a significant measurement error source for longer wavelength SARs at altitudes greater than 200 km such as the Seasat SAR, the Japanese Space Agency's JERS-1 and Phased Array L-Band Synthetic Aperture Radar (PALSAR), or the European TerraSAR system. Users of data from these systems may be faced with an uncertainty in their backscatter measurements greater than any other error source, dependent on the local ionospheric conditions during their particular data-take. This paper seeks to provide a comprehensive set of measures users can refer to, to determine whether a given dataset has been affected by Faraday rotation. Linear single-, dual-, and quad-polarized measurements are considered. The focus is on land, rather than ocean applications.

The paper begins with a discussion of ionospheric effects on electromagnetic waves. Then, the effects of Faraday rotation on linearly polarized scattering matrix measurements are modeled. The model is applied to undistorted scattering matrix measurements to estimate the extent to which common parameters extracted from polarimetric SAR data (e.g., the HH-VV phase difference) will be affected by Faraday rotation. In a companion paper [13], the subject of estimation and correction for a Faraday rotation angle $\mathbf{\Omega}$ is addressed. Finally, the results of the paper are summarized in Section V.

## II. Ionospheric Effects

The ionosphere is defined to be the region of the upper atmosphere with large quantities of charged particles (an ionized medium). This ionized medium becomes anisotropic in the presence of a steady magnetic field such as the earth's magnetic field. Radio waves propagating through the ionosphere, therefore, experience a rotation of polarization vector known as Faraday rotation. The magnitude of the Faraday rotation angle depends on the frequency of the wave and the direction of the earth's magnetic field and its plasma electron density. Since the parameters of the earth's ionosphere are dynamic and their fluctuations depend on diurnal, seasonal, latitudinal, and solar cycle effects, accurate calculation of the Faraday rotation of the polarization vectors is difficult. In the presence of the earth's magnetic field, the ionosphere becomes a birefringent medium with indexes of refraction for left and right circular polarizations given by [23]

$$\mathbf{\Omega} = \frac{K}{f^2} \int NH \cos\theta \sec\chi dh \quad [\text{rad}]. \tag{1}$$

$\mathbf{\Omega}$ is the Faraday rotation angle due to one-way propagation through the ionosphere, where

- $K$ $2.97 \times 10^{-2}$;
- $f$ radio propagation frequency [hertz];
- $N$ electron concentration (per cubic meter);
- $H$ intensity of earth's magnetic field (amperes per meter);
- $\theta$ angle between the normal to the direction of wave propagation and the magnetic field;
- $\chi$ vertical angle of the ray;
- $\sec\chi$dh differential element of the path length (ds).

To determine the Faraday rotation angle $\mathbf{\Omega}$ requires the value of the total electron current (TEC), the value of magnetic field $B$, and the angle $\theta$ between $B$ and the direction of wave propagation.

TABLE I
Estimated Maximum Values for Faraday Rotation Angles for C-Band (6-cm Wavelength), L-Band (24-cm Wavelength), and P-Band (68-cm Wavelength), Under Peak TEC Conditions

| | $\Omega$ (degrees) |
|---|---|
| **C-Band (6 cm)** | 2.5° |
| **L-Band (24 cm)** | 40° |
| **P-Band (68 cm)** | 321° |

To bound the expected effects of Faraday rotation on linearly polarized backscatter signatures, we will use the maximum values for $\Omega$ given in Table I, which correspond to those expected for a spaceborne SAR in a low-earth ($< 1200$ km altitude), polar orbit, observing during the highest anticipated TEC value for solar maximum. The values of $\mathbf{\Omega}$ given in the table should be regarded as upper limits for the actual $\mathbf{\Omega}$ values in each waveband—actual values for $\mathbf{\Omega}$ will generally be lower [14]. Clearly, Faraday rotation effects are expected to be minimal for C-band, but may be significant at L-band and P-band.

One conclusion to be drawn from Table I is that Faraday rotation effects at C-band (and by inference X-band or shorter wavelengths) can largely be ignored. Another is that Faraday rotation effects at P-band may be very significant and could be a major contributor to backscatter measurement error. Faced with such a large potential (one-way) Faraday rotation, most radar designers would opt for circular polarization measurements, as is common in planetary science radars, or look for a way to correct a set of fully polarimetric measurements [13]. At L-band, the upper limit on $\mathbf{\Omega}$ of $\sim 40°$ means that Faraday rotation may be a significant source of measurement error under certain conditions. At least one author [11] has suggested that Faraday rotations may be as great as 90°, though [12] places an upper limit on $\mathbf{\Omega}$ of 30°. In what follows, we will examine the effects of Faraday rotations between $\mathbf{\Omega} = 0°$ and $\mathbf{\Omega} = 90°$.

## III. Modeling the Effect on Backscatter Signatures

Under the assumption that there is no variation of Faraday rotation across the SAR antenna beam, linearly polarized waves transmitted and received by the SAR system can experience two instances of Faraday rotation, in propagating downward then upward. The sense of Faraday rotation in each direction is the same relative to the earth's magnetic field and is independent of the propagation direction. For a general case, assume the transmitted electric field, $\mathbf{E}_\mathrm{t}$ can be represented in terms of horizontal and vertical field components. After one-way transmission through the ionosphere, the field incident $\mathbf{B}$ on the earth's surface is rotated by the Faraday rotation matrix $\mathbf{R_F}$ such that $\mathbf{E}_\mathrm{i} = \mathbf{R_F}\mathbf{E}_\mathrm{t}$. The scattered field from the target (distributed target in case of land surface) undergoes another rotation along the receive propagation path before reaching the antenna. Therefore, the elements of the scattering matrix $\mathbf{S}$ of the target are modified as a result of the round-trip Faraday rotation angle. For a SAR system measuring linear horizontal (H) and vertical (V)

polarizations in the antenna coordinate system, the measured scattering matrix $\mathbf{M}$ can be written (after [4] and [6]) as

$$\mathbf{M} = \mathrm{A}e^{\mathrm{j}\phi}\mathbf{R}^{\mathbf{T}}\mathbf{R}_{\mathbf{F}}\mathbf{S}\mathbf{R}_{\mathbf{F}}\mathbf{T} + \mathbf{N} \tag{2}$$

where $\mathbf{S}$ is the scattering matrix, $\mathbf{R}_{\mathbf{F}}$ represents the one-way Faraday rotation matrix, $\mathbf{R}$ is the receive distortion matrix (of the radar system), and $\mathbf{T}$ is the transmit distortion matrix (of the radar system). Both $\mathbf{R}$ and $\mathbf{T}$ can include crosstalk and channel amplitude and phase imbalance terms. The (real) factor A represents the overall gain of the radar system, and the complex factor $e^{\mathrm{j}\phi}$ represents the round-trip phase delay and system-dependent phase effects on the signal. The matrix $\mathbf{N}$ represents additive noise terms present in each measurement due to earth radiation, thermal fluctuations in the receiver, and digitization noise.

Calibration techniques have been described (e.g., [15]) that can successfully estimate and correct for the system-dependent terms A, $\mathbf{R}$, and $\mathbf{T}$. Assume for the moment that the system under consideration is either so well-calibrated that A, $\mathbf{R}$ and $\mathbf{T}$ can be ignored or sufficiently stable that estimates for A, $\mathbf{R}$, and $\mathbf{T}$ obtained when no Faraday rotation is present can be applied to measurements obtained when Faraday rotation is present. The complex term $e^{\mathrm{j}\phi}$ is usually ignored except in the case of interferometric data analysis. If the SNR is high enough, the additive noise terms in $\mathbf{N}$ can also be ignored, for now. Making these assumptions, (2) becomes simply

$$\mathbf{M} = \mathbf{R}_{\mathbf{F}}\mathbf{S}\mathbf{R}_{\mathbf{F}}. \tag{3}$$

Equation (3) can be expanded to show the nature of the problem when Faraday rotation alone is the measurement error source

$$\begin{bmatrix} M_{\mathrm{hh}} & M_{\mathrm{vh}} \\ M_{\mathrm{hv}} & M_{\mathrm{vv}} \end{bmatrix} = \begin{bmatrix} \cos\Omega & \sin\Omega \\ -\sin\Omega & \cos\Omega \end{bmatrix} \cdot \begin{bmatrix} S_{\mathrm{hh}} & S_{\mathrm{vh}} \\ S_{\mathrm{hv}} & S_{\mathrm{vv}} \end{bmatrix} \begin{bmatrix} \cos\Omega & \sin\Omega \\ -\sin\Omega & \cos\Omega \end{bmatrix}. \tag{4}$$

Note that the backward scattering alignment (BSA) convention is assumed here. Equation (4) can be written

$$M_{\mathrm{hh}} = S_{\mathrm{hh}}\cos^2\Omega - S_{\mathrm{vv}}\sin^2\Omega + (S_{\mathrm{hv}} - S_{\mathrm{vh}})\sin\Omega\cos\Omega \tag{5a}$$

$$M_{\mathrm{vh}} = S_{\mathrm{vh}}\cos^2\Omega + S_{\mathrm{hv}}\sin^2\Omega + (S_{\mathrm{hh}} + S_{\mathrm{vv}})\sin\Omega\cos\Omega \tag{5b}$$

$$M_{\mathrm{hv}} = S_{\mathrm{hv}}\cos^2\Omega + S_{\mathrm{vh}}\sin^2\Omega - (S_{\mathrm{hh}} + S_{\mathrm{vv}})\sin\Omega\cos\Omega \tag{5c}$$

$$M_{\mathrm{vv}} = S_{\mathrm{vv}}\cos^2\Omega - S_{\mathrm{hh}}\sin^2\Omega + (S_{\mathrm{hv}} - S_{\mathrm{vh}})\sin\Omega\cos\Omega. \tag{5d}$$

Invoking backscatter reciprocity, i.e., $S_{\mathrm{hv}} = S_{\mathrm{vh}}$,

$$M_{\mathrm{hh}} = S_{\mathrm{hh}}\cos^2\Omega - S_{\mathrm{vv}}\sin^2\Omega \tag{6a}$$

$$M_{\mathrm{vh}} = S_{\mathrm{hv}} + (S_{\mathrm{hh}} + S_{\mathrm{vv}})\sin\Omega\cos\Omega \tag{6b}$$

$$M_{\mathrm{hv}} = S_{\mathrm{hv}} - (S_{\mathrm{hh}} + S_{\mathrm{vv}})\sin\Omega\cos\Omega \tag{6c}$$

$$M_{\mathrm{vv}} = S_{\mathrm{vv}}\cos^2\Omega - S_{\mathrm{hh}}\sin^2\Omega. \tag{6d}$$

Note that for cross-pol measurements, the presence of nonzero Faraday rotation means that they will not necessarily be reciprocal, i.e., $M_{\mathrm{hv}} \neq M_{\mathrm{vh}}$.

### A. HH Polarization Measurements Only

Several spaceborne SARs have been flown that measure L-band HH polarization backscatter only, i.e., Seasat SAR, SIR-A, SIR-B, and JERS-1. The radar cross section measured by these radars in the presence of Faraday rotation is (omitting a factor of $4\pi$ for simplicity)

$$M_{\mathrm{hh}}M_{\mathrm{hh}}^* = S_{\mathrm{hh}}S_{\mathrm{hh}}^*\cos^4\Omega - 2\mathrm{Re}\,(S_{\mathrm{hh}}S_{\mathrm{vv}}^*)\sin^2\Omega\cos^2\Omega + S_{\mathrm{vv}}S_{\mathrm{vv}}^*\sin^4\Omega. \tag{7}$$

We can also model the effect of Faraday rotation on repeat-pass interferometry measurements made by HH-pol only spaceborne radars. This is done by correlating an initial measurement of $S_{\mathrm{hh}}$ with zero rotation with a second measurement that has Faraday rotation as in (6), to give

$$M_{\mathrm{hh}_1}M_{\mathrm{hh}_2}^* = S_{\mathrm{hh}_1}S_{\mathrm{hh}_2}^*\cos^2\Omega - S_{\mathrm{hh}_1}S_{\mathrm{vv}_2}^*\sin^2\Omega. \tag{8}$$

Assuming no change in the backscatter, i.e., that there is no temporal decorrelation, we can assess the decorrelation introduced by Faraday rotation alone

$$M_{\mathrm{hh}_1}M_{\mathrm{hh}_2}^* = S_{\mathrm{hh}}S_{\mathrm{hh}}^*\cos^2\Omega - S_{\mathrm{hh}}S_{\mathrm{vv}}^*\sin^2\Omega. \tag{9}$$

As a normalized correlation coefficient, this can be expressed as

$$\rho_{\mathrm{Faraday}} = \frac{\left|\langle M_{\mathrm{hh}_1}M_{\mathrm{hh}_2}^*\rangle\right|}{\sqrt{\langle M_{\mathrm{hh}_1}M_{\mathrm{hh}_1}^*\rangle\langle M_{\mathrm{hh}_2}M_{\mathrm{hh}_2}^*\rangle}}$$

or as in (10), shown at at the bottom of the page, where $\langle\cdot\rangle$ denotes expected value. This correlation coefficient does not include temporal decorrelation or noise decorrelation.

### B. Dual-Polarized (HH and HV) Measurements

A dual-polarized radar may provide only HH and HV backscatter measurements, which allows for wider swaths to be illuminated than fully polarimetric modes because of lower data rates. This type of data collection was implemented on the SIR-C radar and has also been proposed for planned spaceborne SARs such as the Japanese Space Agency's PALSAR and the European TerraSAR. Forming cross products between the appropriate scattering matrix terms in (6), and averaging over a homogeneous area to approximate the expected value, for dual-polarized measurements in the presence of Faraday rotation we obtain

$$\langle M_{\mathrm{hh}}M_{\mathrm{hh}}^*\rangle = \langle S_{\mathrm{hh}}S_{\mathrm{hh}}^*\rangle\cos^4\Omega - 2\langle\mathrm{Re}\,\{S_{\mathrm{hh}}S_{\mathrm{vv}}^*\}\rangle \cdot \sin^2\Omega\cos^2\Omega + \langle S_{\mathrm{vv}}S_{\mathrm{vv}}^*\rangle\sin^4\Omega \tag{11a}$$

$$\langle M_{\mathrm{hv}}M_{\mathrm{hv}}^*\rangle = \langle S_{\mathrm{hv}}S_{\mathrm{hv}}^*\rangle + \sin^2\Omega\cos^2\Omega \cdot (\langle S_{\mathrm{hh}}S_{\mathrm{hh}}^*\rangle + \langle S_{\mathrm{vv}}S_{\mathrm{vv}}^*\rangle + 2\langle\mathrm{Re}\,\{S_{\mathrm{hh}}S_{\mathrm{vv}}^*\}\rangle) \tag{11b}$$

$$\rho_{\mathrm{Faraday}} = \frac{\left|\langle S_{\mathrm{hh}}S_{\mathrm{hh}}^*\cos^2\Omega - S_{\mathrm{hh}}S_{\mathrm{vv}}^*\sin^2\Omega\rangle\right|}{\sqrt{\langle S_{\mathrm{hh}}S_{\mathrm{hh}}^*\rangle\langle S_{\mathrm{hh}}S_{\mathrm{hh}}^*\cos^4\Omega - 2\mathrm{Re}\,(S_{\mathrm{hh}}S_{\mathrm{vv}}^*)\sin^2\Omega\cos^2\Omega + S_{\mathrm{vv}}S_{\mathrm{vv}}^*\sin^4\Omega\rangle}} \tag{10}$$

TABLE II
L-BAND BACKSCATTER MEASUREMENTS FROM NASA/JPL AIRSAR DATA FOR A VARIETY OF LAND COVER TYPES

| L-Band | HH $\sigma^\circ$ (dB) | HV $\sigma^\circ$ (dB) | VV $\sigma^\circ$ (dB) | HH-VV Phase (deg.) | HH-VV Correlation |
|---|---|---|---|---|---|
| Bare Soil | -16.5 | -26.9 | -14.7 | -23.7 | 0.75 |
| Pasture | -13.3 | -25 | -11.8 | -18.6 | 0.75 |
| Upland Forest | -9.2 | -14.3 | -9.4 | 7.9 | 0.25 |
| Swamp Forest | -6.9 | -14.5 | -7.3 | 165.4 | 0.06 |
| Plantation | -8 | -15.7 | -9.7 | 52.1 | 0.12 |
| Conifers | -6.2 | -13.1 | -8.9 | 36.9 | 0.21 |

$$\langle M_{\rm hh}M_{\rm hv}^*\rangle = \sin\Omega\cos\Omega\left(-\langle S_{\rm hh}S_{\rm hh}^*\rangle\cos^2\Omega - \langle S_{\rm hh}S_{\rm vv}^*\rangle \cdot cos^2\Omega - \langle S_{\rm vv}S_{\rm hh}^*\rangle\sin^2\Omega + \langle S_{\rm vv}S_{\rm vv}^*\rangle\sin^2\Omega\right) \tag{11c}$$

where we have assumed that reflection symmetry holds, as is the case for many natural targets, with the consequence that

$$\langle S_{\rm hh}S_{\rm hv}^*\rangle = \langle S_{\rm hv}S_{\rm vv}^*\rangle = 0. \tag{12}$$

### C. Quad-Polarized Measurements

Fully polarimetric or quad-pol backscatter measurements were collected during the SIR-C mission and are planned for TerraSAR-L and as an experimental mode for PALSAR. Expressions for the cross products generated from fully polarimetric data are easily generated from the appropriate terms in (6) by averaging over a homogeneous area to approximate the expected value

$$\langle M_{\rm hh}M_{\rm hh}^*\rangle = \langle S_{\rm hh}S_{\rm hh}^*\rangle\cos^4\Omega - 2\langle{\rm Re}\{S_{\rm hh}S_{\rm vv}^*\}\rangle \cdot\sin^2\Omega\cos^2\Omega + \langle S_{\rm vv}S_{\rm vv}^*\rangle\sin^4\Omega \tag{13a}$$

$$\langle M_{\rm hv}M_{\rm hv}^*\rangle = \langle S_{\rm hv}S_{\rm hv}^*\rangle + [\langle S_{\rm hh}S_{\rm hh}^*\rangle + \langle S_{\rm vv}S_{\rm vv}^*\rangle + 2\langle{\rm Re}\{S_{\rm hh}S_{\rm vv}^*\}\rangle]\sin^2\Omega\cos^2\Omega \tag{13b}$$

$$\langle M_{\rm vh}M_{\rm vh}^*\rangle = \langle M_{\rm hv}M_{\rm hv}^*\rangle \tag{13c}$$

$$\langle M_{\rm vv}M_{\rm vv}^*\rangle = \langle S_{\rm hh}S_{\rm hh}^*\rangle\sin^4\Omega - 2\langle{\rm Re}\{S_{\rm hh}S_{\rm vv}^*\}\rangle \cdot\sin^2\Omega\cos^2\Omega + \langle S_{\rm vv}S_{\rm vv}^*\rangle\cos^4\Omega \tag{13d}$$

$$\langle M_{\rm hv}M_{\rm vh}^*\rangle = \langle S_{\rm hv}S_{\rm hv}^*\rangle - [\langle S_{\rm hh}S_{\rm hh}^*\rangle + \langle S_{\rm vv}S_{\rm vv}^*\rangle + 2\langle{\rm Re}\{S_{\rm hh}S_{\rm vv}^*\}\rangle]\sin^2\Omega\cos^2\Omega \tag{13e}$$

$$\langle M_{\rm hh}M_{\rm vv}^*\rangle = \langle S_{\rm hh}S_{\rm vv}^*\rangle\cos^4\Omega - (\langle S_{\rm hh}S_{\rm hh}^*\rangle + \langle S_{\rm vv}S_{\rm vv}^*\rangle) \cdot\sin^2\Omega\cos^2\Omega + \langle S_{\rm vv}S_{\rm hh}^*\rangle\sin^4\Omega \tag{13f}$$

$$\langle M_{\rm hh}M_{\rm hv}^*\rangle = -[\langle S_{\rm hh}S_{\rm hh}^*\rangle + \langle S_{\rm hh}S_{\rm vv}^*\rangle]\sin\Omega\cos^3\Omega + [\langle S_{\rm vv}S_{\rm hh}^*\rangle + \langle S_{\rm vv}S_{\rm vv}^*\rangle]\sin^3\Omega\cos\Omega \tag{13g}$$

$$\langle M_{\rm hh}M_{\rm vh}^*\rangle = -\langle M_{\rm hh}M_{\rm hv}^*\rangle \tag{13h}$$

$$\langle M_{\rm vv}M_{\rm hv}^*\rangle = -[\langle S_{\rm vv}S_{\rm hh}^*\rangle + \langle S_{\rm vv}S_{\rm vv}^*\rangle]\sin\Omega\cos^3\Omega + [\langle S_{\rm hh}S_{\rm hh}^*\rangle + \langle S_{\rm hh}S_{\rm vv}^*\rangle]\sin^3\Omega\cos\Omega \tag{13i}$$

$$\langle M_{\rm vv}M_{\rm vh}^*\rangle = -\langle M_{\rm vv}M_{\rm hv}^*\rangle \tag{13j}$$

where again it is assumed that reflection symmetry holds.

## IV. MODEL RESULTS

To accurately determine what will happen to backscatter measurements affected by Faraday rotation, it is clear that the full scattering matrix or covariance matrix should be known. The polarimetric backscatter measurements in Table II were extracted from L-band polarimetric SAR data collected by the National Aeronautics and Space Administration Jet Propulsion Laboratory (NASA/JPL) Airborne SAR (AIRSAR) system over a tropical rain forest in Belize during 1991 and over a site in Raco, MI, in June 1991. For these data, Faraday rotation is definitely *not* a problem, since they were collected at an altitude of less than 10 km, well below the active layers of the ionosphere. They are presented here as typical of scattering from natural terrain with reflection symmetry (like- and cross-pol correlations are negligible). Backscatter models that approximate the measurements in Table II are given in Appendix I, and a special case where reflection symmetry may not hold because of local azimuth slopes is considered in Appendix II. The behavior of the scattering from bare soil is representative of scattering observed from similar fields around the world, for example. The scattering behavior for pasture is typical of grassland areas; the upland forest signature is representative of broadleaf forests in other areas; the swamp forest is an example of a forest with significant double-bounce as well as canopy scatter, because of flooding beneath the canopy; and the plantation and conifer areas are different examples of forests that exhibit significant double-bounce, as well as canopy scatter because of a relatively sparse canopy, which is more transparent to longer wavelength radar waves.

The effects of Faraday rotation on the measurements given in Table II will be plotted for various backscatter measurements as a function of the Faraday rotation angle $\mathbf{\Omega}$, over the range $0^\circ$ to $180^\circ$. It is not necessary to plot over a larger range of $\mathbf{\Omega}$, since it is quite easy to show that

$$\mathbf{M}(\Omega) = \mathbf{R_F}(\Omega)\,\mathbf{S}\,\mathbf{R_F}(\Omega) = \mathbf{M}(\Omega \pm \pi). \tag{16}$$

### A. HH Polarization Measurements Only

The L-band polarimetric backscatter measurements given in Table II were inserted into (7) in order to estimate the effect on measurements made by a radar capable only of transmitting and receiving H-polarized waves. The results are shown in Fig. 1.

Referring to Table I, the maximum Faraday rotation angle expected for an L-band spaceborne radar system is $\sim 40^\circ$. From Fig. 1, it is clear that a Faraday rotation angle of this magnitude will lead to a significant drop in the measured backscatter level for all scatterer types. There is some variation in the HH backscatter measurement due to the different polarization signatures over the full range of Faraday rotation angles, but no very significant differences between the different scattering types over the range $0^\circ$ to $40^\circ$. Thus, at L-band we would expect the most visible effect of Faraday rotation to be a general lowering in the measured backscatter, by as much as 3 or 4 dB, comparing results at $0^\circ$ rotation to those at about $40^\circ$. Comparing data-takes with Faraday rotation and without Faraday rotation over similar areas, the most noticeable effect would be a drop in overall SNR in the former case (assuming that the noise level is the same in each case).

Another measure of interest is the dynamic range (DR) in the data, defined as the ratio of the highest measured backscatter value in the image to the lowest. In a scene containing just the backscatter types in Table II, the behavior of this measure of dynamic range should be similar to that shown in Fig. 2. Each measurement in this case is assumed to be the backscatter plus an additive noise at various levels. For a noise-equivalent sigma-zero

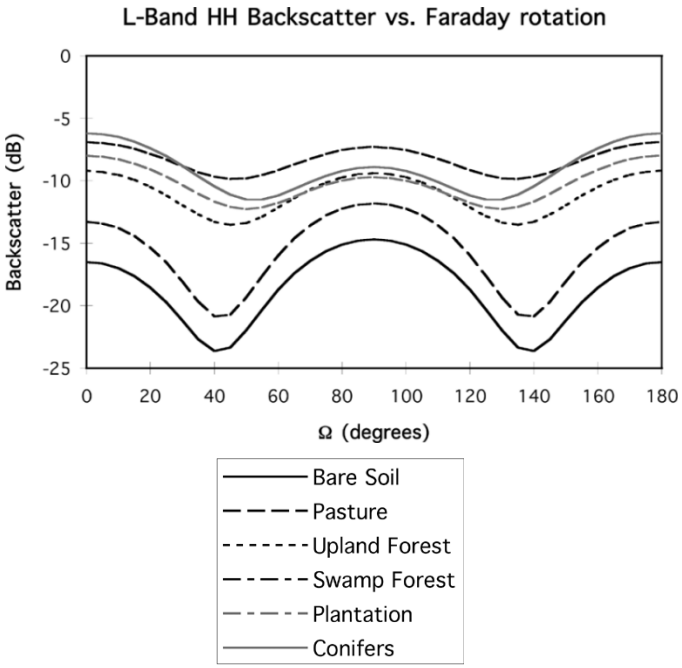


Fig. 1. Predicted measured backscatter values in the presence of uncompensated Faraday rotation $\mathbf{\Omega}$ as measured by an L-band H-transmit, H-receive radar for different backscatter types.

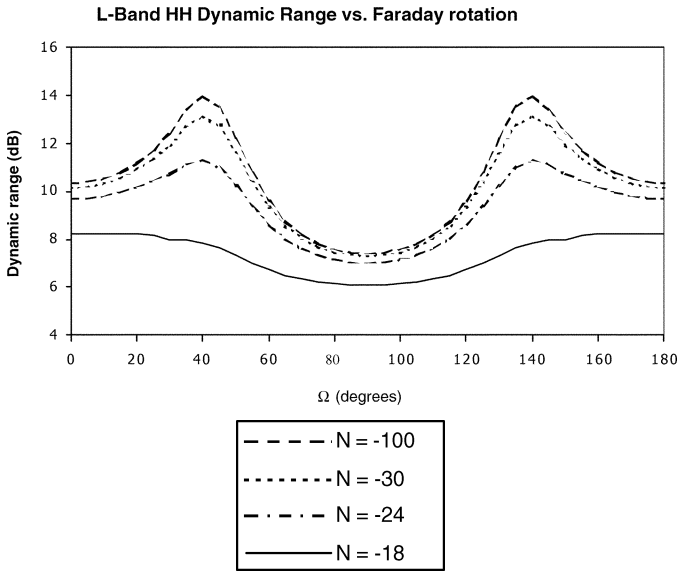


Fig. 2. Predicted values of the dynamic range as measured by an L-band H-transmit, H-receive radar for the backscatter types in Table II as a function of Faraday rotation angle $\mathbf{\Omega}$. The four curves plotted correspond to different values of the noise-equivalent sigma-zero $N$, between $N = -18$ dB and $N = -100$ dB.

($N$) of $-100$ dB, for example, the additive noise should be negligible. Noise levels of $-24$ and $-18$ dB are representative of the specified and actual performance of the JERS-1 SAR. SIR-C L-band data had a noise floor below $-30$ dB, and as low as $-50$ dB for some data-takes. In this case, the dynamic range is expected to increase significantly as the Faraday rotation increase from $0°$ to $40°$. As higher noise levels are introduced, this effect is masked. At $\mathbf{\Omega} = 90°$, the dynamic range is significantly reduced in all cases, as suggested in [11].

The effect of Faraday rotation on repeat-pass Interferometry measurements made by an L-band spaceborne SAR has also been modeled using expression (10). A noise floor level of $-30$ dB was included in the denominator of the calculated correlation coefficients: thus the correlation is never identical to unity, even when the ionosphere has no effect (case $\mathbf{\Omega} = 0$). (As was the case in the discussion of dynamic range, higher levels of system noise may mask some of the effects on the correlation attributable to Faraday rotation.) Temporal decorrelation due to changes in physical characteristics have not been included for any of the backscatter types. It can be seen from Fig. 3 that the correlation coefficients are not much affected by Faraday rotation up to $\mathbf{\Omega} = 30°$, but then drop off markedly for larger angles. For $\mathbf{\Omega} > 30°$, the correlation coefficients show significant variations across target types, with forested areas exhibiting higher correlation than nonforested areas. For $\mathbf{\Omega} = 90°$, the correlation coefficient is actually the same as the HH-VV correlation coefficient, as can be seen by comparing the values in Fig. 3 with the appropriate column in Table II. Thus, the effect of Faraday rotation may be noticeable in repeat-pass interferometry data as a general decrease in the temporal correlation coefficients, and if $\mathbf{\Omega}$ is close to $90°$, high values for the correlation coefficient may be observed in nonforested areas, and low correlation coefficient values in forested areas.

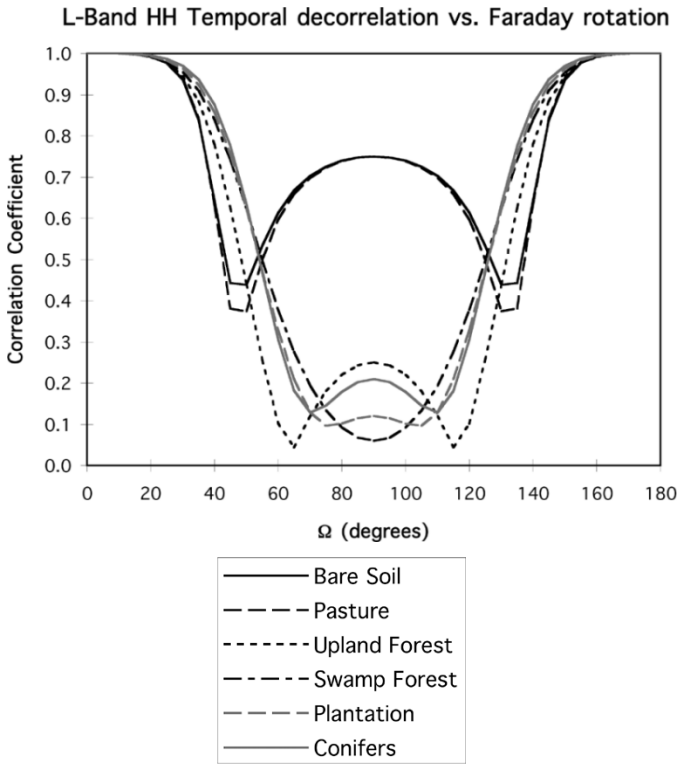


Fig. 3. Modeled correlation coefficients for nominally HH polarization repeat-pass measurements of the different backscatter types from Table II, including decorrelation due to system noise at $-30$ dB and Faraday rotation angle $\mathbf{\Omega}$.

### *B. Dual-Polarized (HH and HV) Measurements*

If only HH and HV measurements are available, we can look at the behavior of the measured "HV" backscatter values and the measured "HH-HV" correlation coefficient with Faraday rotation angle, as estimated from (11). These are shown in Figs. 4

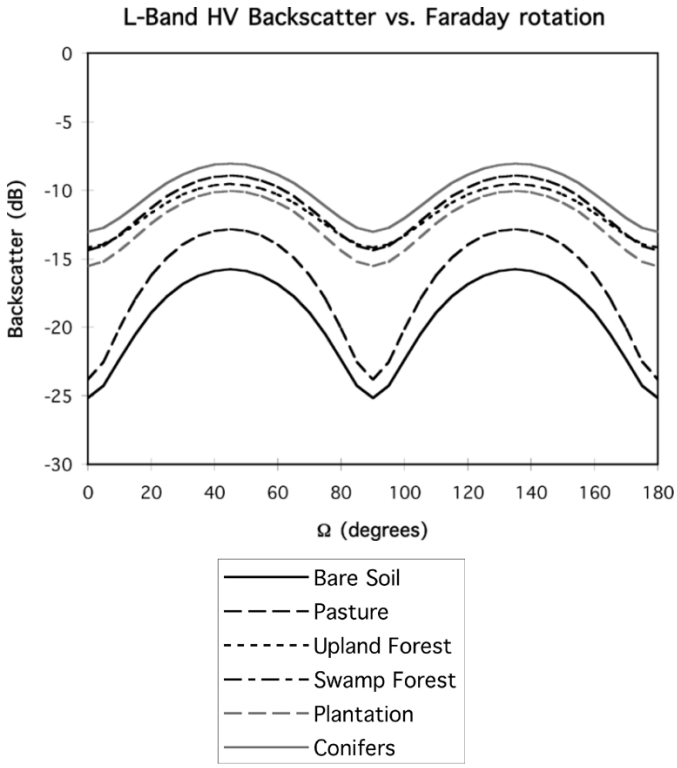


Fig. 4. Predicted measured backscatter values in the presence of uncompensated Faraday rotation $\mathbf{\Omega}$ as measured by an L-band H-transmit, V-receive radar for different backscatter types.

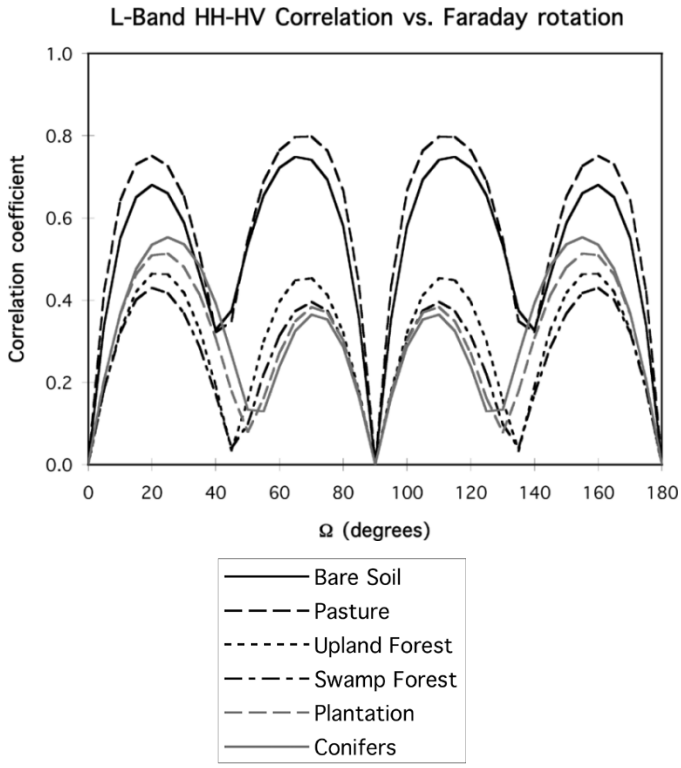


Fig. 5. Modeled L-band "HH-HV" correlation coefficient measurement (dual-polarized data) versus Faraday rotation angle $\mathbf{\Omega}$ for the different backscatter types from Table II.

and 5. The correlation coefficients were estimated using a noise floor of $-30$ dB. The cyclic behavior visible in Fig. 4 stems from the $(\sin 2\mathbf{\Omega})^2$ dependence of the like-pol contributions to the "HV" backscatter measurement in (11b), which are maximum for $\mathbf{\Omega} = 45°$. Comparing Figs. 4 and 1, we see that it is possible to have the nominal HV backscatter measurement be larger than the nominal HH backscatter measurement, e.g., for $\mathbf{\Omega} \approx 45°$. This situation almost never occurs due to scattering in nature, so should be simple to detect in the data.

The null visible in the HH-HV correlation values plotted in Fig. 5 at $\mathbf{\Omega} = 90°$ stems from the $\sin 2\mathbf{\Omega}$ dependence of the "HH-HV" correlation measurement in (11c). There is also a less pronounced null at around $\mathbf{\Omega} = 45°$. The figure indicates that for targets that have reflection symmetry, a small Faraday rotation angle of $< 20°$ should be detectable as a nonzero "HH-HV" correlation coefficient, which is usually close to zero for such scatterers. Except for $\mathbf{\Omega} = 0°, 90°,$ or $, 180°$, the HH-HV correlation coefficient will also exhibit significant differences depending on the type of scatterer, especially between forested/nonforested areas.

### C. Quad-Polarized Measurements

Returning to (13e), the expected value of the $M_{\rm hv}M_{\rm vh}{}^*$ term is a real number, which can take both positive and negative values. We can plot the phase of the nominal phase difference between HV and VH as a function of Faraday rotation angle, as in Fig. 6. This phase difference can only takes two values, 0 and $\pm 180°$. For small values of $\mathbf{\Omega}$, the phase of $M_{\rm hv}M_{\rm vh}{}^*$ is zero for all scatterers. This quickly flips to $180°$ (i.e., the HVVH* term becomes negative) as $\mathbf{\Omega}$ increases, then flips to zero again close to $90°$ and then cycles once more as $\mathbf{\Omega}$ goes from $90°$ to $180°$. Thus, a relatively small Faraday rotation angle may be detectable as a $180°$ phase change in the $M_{\rm hv}M_{\rm vh}{}^*$ term.

| | |
|---|---|
| Upland Forest | 00000ππππππππππ000000000ππππππππππ00000 |
| Conifers | 00000ππππππππππ000000000ππππππππππ00000 |
| Plantation | 0000ππππππππππππ0000000ππππππππππππ0000 |
| Swamp Forest | 0000ππππππππππππ0000000ππππππππππππ0000 |
| Pasture | 00ππππππππππππππππ000ππππππππππππππππ00 |
| Bare soil | 00ππππππππππππππππ000ππππππππππππππππ00 |
| Ω (deg.) | 0 90 180 |

Fig. 6. Modeled L-band "$M_{\rm hv}M_{\rm vh}{}^*$" phase transitions (0 or $\pi$) versus Faraday rotation angle $\mathbf{\Omega}$ for the different backscatter types in Table II.

The behavior of the measured phase difference between HH and VV versus Faraday rotation was modeled using (13f). The results are clearly backscatter-dependent, as can be seen in Fig. 7. For the swamp forest, the measured phase difference hardly changes at all, while for the bare soil, pasture, and upland forest, the measured phase difference cycles through $360°$ over the range of $\mathbf{\Omega}$.

The behavior of the measured "HHVV*" correlation coefficient versus Faraday rotation was also modeled by forming a correlation coefficient from the appropriate terms in (13). The results are shown in Fig. 8. The plots all show a pronounced peak in the correlation at $\mathbf{\Omega} = 45°$. Returning to (6a) and (6d), we can see that the nominally "HH" and "VV" backscatter measurements will be identical for $\mathbf{\Omega} = 45°$ and $135°$, hence the high value for the correlation coefficient.

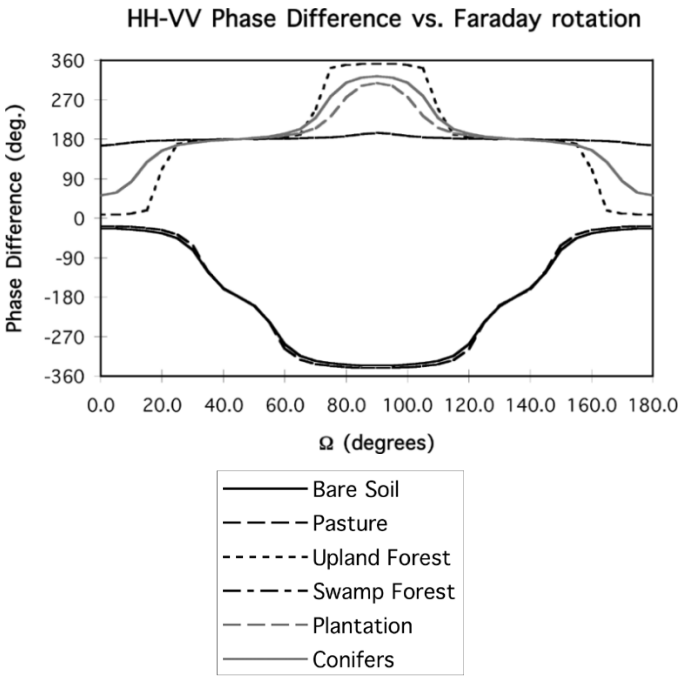


Fig. 7. Modeled L-band phase difference between HH and VV versus Faraday rotation angle $\mathbf{\Omega}$ for the different backscatter types in Table II.

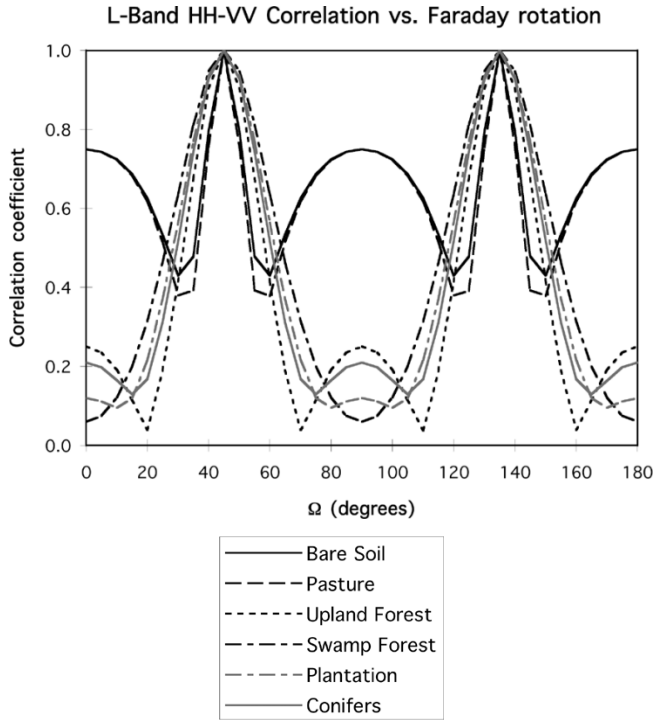


Fig. 8. Modeled L-band "HHVV$^*$" correlation measurements versus Faraday rotation angle $\mathbf{\Omega}$ for the different backscatter types from Table II.

Finally, the model results for a nominal "VV" backscatter measurement versus Faraday rotation angle are shown in Fig. 9. The results are similar to those in Fig. 1 for "HH" measurements. The most notable feature seen in comparing the plots shown in Figs. 9 and 1 is the way that the HH and VV measurements "trade places" for $\mathbf{\Omega} = 90°$.

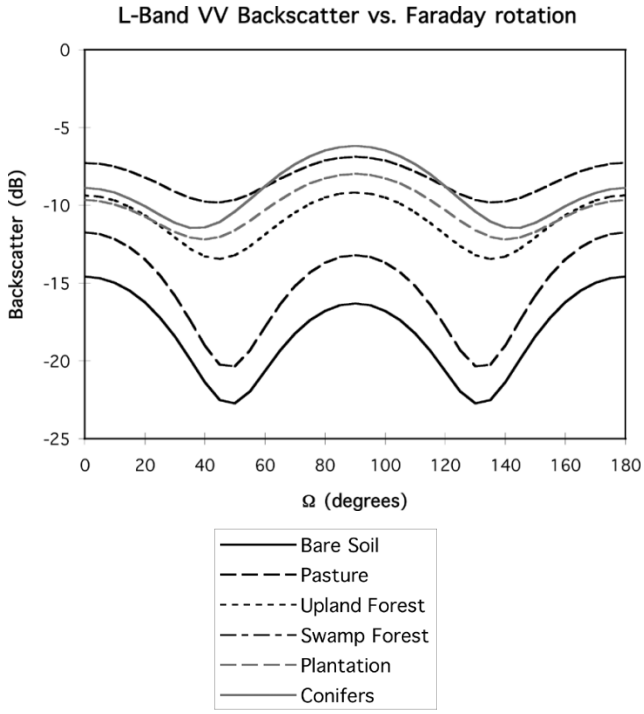


Fig. 9. Modeled L-band backscatter for a nominally VV polarized measurement versus Faraday rotation angle $\mathbf{\Omega}$ for the different backscatter types in Table II.

## V. Summary and Discussion

The effects of Faraday rotation on spaceborne L-band SAR backscatter signatures have been modeled, and the detection of Faraday rotation in actual data has been discussed. This section addresses the problem of determining whether Faraday rotation is present in a given set of measured data. Our simulation results are summarized for each type of measurement in Tables III and IV.

To determine whether a given dataset has been subject to Faraday rotation, it is necessary to have for comparison either a reference dataset collected by the same radar system from an identical viewing geometry and zero Faraday rotation, or an accurate understanding of the scattering behavior of the terrain under investigation. Then, measurements from the current dataset can be compared against the reference data. The results in Table III suggest that the most sensitive indicators of the presence of relatively small Faraday rotations ($\mathbf{\Omega} \leq 20°$) are the behavior of the HV backscatter and the HHHV$^*$ correlation coefficient, which show significant differences from their values at $\mathbf{\Omega} = 0$. For $\mathbf{\Omega} \sim 40°$ there are many indicators. As $\mathbf{\Omega}$ approaches $90°$, the HV measurements are unchanged, and the HH and VV measurements are essentially switched. The best indicator at $\mathbf{\Omega} = 90°$ would appear to be to look for a change in the sign of the HH to VV phase difference.

In the case of single-polarized (HH) measurements, as made by the Japanese JERS-1 satellite, the effects of Faraday rotation should show up primarily as a significant drop in SNR and a radiometric calibration error. In the case of repeat-pass interferometry data, it may also be detected as a change in the scene-to-scene correlation or in the behavior of certain known

TABLE III
SUMMARY OF KEY INDICATORS OF THE PRESENCE OF FARADAY ROTATION IN L-BAND SAR DATA MODELED USING DATA FROM TABLE II ASSUMES NE Sigma-Zero $= -30$ dB. CHANGES INDICATED ARE RELATIVE TO THE VALUE FOR THAT PARAMETER WHEN $\mathbf{\Omega} = 0$ (GIVEN IN TABLE II). THE RANGE OF VALUES GIVEN INDICATES THE BEHAVIOR ACROSS THE SET OF SCATTERERS GIVEN IN TABLE II. $\rho$ MEANS CORRELATION COEFFICIENT. $\Delta\phi$ MEANS PHASE DIFFERENCE

| Measure | $\Omega = 3$ | $\Omega = 5$ | $\Omega = 10$ | $\Omega = 20$ | $\Omega = 40$ | $\Omega = 90$ |
|---|---|---|---|---|---|---|
| $\Delta\sigma^o$(HH) - dB | 0 | −0.1 | −0.2 –> −0.5 | −0.9 –> −1.9 | −2.7 –> −7.2 | −2.7 –> +1.7 |
| $\Delta\sigma^o$(VV) - dB | 0 | −0.1 | −0.2 –> −0.5 | −0.9 –> −1.8 | −1.8 –> −7.3 | −1.7 –> +2.7 |
| $\Delta\sigma^o$(HV) - dB | +0.1 –> +0.5 | +0.3 –> +0.7 | +1.0 –> +3.7 | +2.6 –> +7.6 | +4.6 –> +10.8 | 0 |
| $\Delta\rho(HH_1HH_2^*)$ | 0 | 0 | 0 –> -0.01 | 0 –> -0.03 | -0.15 –> -0.42 | -0.24 –> -0.87 |
| $\Delta\rho$(HHHV*) | +0.11 –> +0.27 | +0.18 –> +0.42 | +0.32 –> +0.64 | +0.43 –> +0.75 | +0.17 –> +0.39 | 0 |
| $\Delta\rho$(HHVV*) | 0 –> −0.01 | −0.02 –> +0.01 | −0.06 –> +0.06 | −0.21 –> +0.25 | −0.13 –> +0.87 | 0 |
| $\Delta\phi$ (HV-VH) - deg | 0 | 0 | 0 or 180 | 0 or 180 | 180 | 0 |
| $\Delta\phi$ (HH-VV) - deg | −0.2 –> +2.2 | −0.5 –> +6.4 | −2.1 –> +31.6 | −11.0 –> +102.4 | −143 –> +171.2 | $= -\phi(\text{HH-VV*})\vert_{\Omega=0}$ |

TABLE IV
DYNAMIC RANGE FOR THE DATA IN TABLE II ESTIMATED FOR DIFFERENT VALUES OF $\mathbf{\Omega}$. ASSUMES NE Sigma-Zero $= -30$ dB

| Measure | $\Omega = 0$ | $\Omega = 3$ | $\Omega = 5$ | $\Omega = 10$ | $\Omega = 20$ | $\Omega = 40$ | $\Omega = 90$ |
|---|---|---|---|---|---|---|---|
| $\sigma^o$(HH) - dB | 10.1 | 10.1 | 10.2 | 10.3 | 10.9 | 13.1 | 7.3 |
| $\sigma^o$(VV) - dB | 7.3 | 7.3 | 7.3 | 7.5 | 8.0 | 1.6 | 10.1 |
| $\sigma^o$(HV) - dB | 12.2 | 11.9 | 11.5 | 10.3 | 8.7 | 7.7 | 12.2 |

TABLE V
EFFECTS OF AZIMUTH TILT ON POLARIZATION SIGNATURES FROM TABLE II. CHANGES INDICATED ARE RELATIVE TO THE VALUE FOR $\theta = 0$

| Measure | $\theta = 3$ | $\theta = 5$ | $\theta = 10$ | $\theta = 20$ | $\theta = 40$ |
|---|---|---|---|---|---|
| $\Delta\sigma^o$(HH) - dB | – | – | 0 –> −0.2 | 0 –> −0.7 | −0.3 –> −1.9 |
| $\Delta\sigma^o$(VV) - dB | – | – | 0 –> −0.2 | 0 –> −0.7 | −0.2 –> −1.6 |
| $\Delta\sigma^o$(HV) - dB | 0 –> 0.1 | 0 –> 0.2 | 0.1 –> 0.9 | 0.3 –> 2.5 | 0.7 –> 4.6 |
| $\Delta\rho$(HHHV*) | 0.01 –> 0.09 | 0.02 –> 0.14 | 0.04 –> 0.25 | 0.07 –> 0.35 | 0.05 –> 0.45 |
| $\Delta\rho$(HHVV*) | – | −0.01 –> 0.0 | −0.04 –> 0.02 | 0.03 –> 0.10 | 0.09 –> 0.38 |
| $\Delta\phi$ (HH-VV) - deg | −1.2 –> 0.1 | −3.3 –> 0.4 | −24.6 –> 1.6 | −157.7 –> 6.0 | −164.9 –> 19.8 |

scatterers, though this may be difficult to separate from other, scene-dependent changes. In dual-polarized measurements, examination of the relative strength of the "HH" and "HV" backscatter measurements and/or the magnitude of the HH to HV correlation coefficient may reveal the presence of Faraday rotation for targets under some circumstances. For quad-polarized data, in addition to the above indicators, a $180^\circ$ phase change in the argument of the $M_{\text{hv}}M_{\text{vh}}$ term should also reveal the presence of Faraday rotation (for $\mathbf{\Omega} \leq 45^\circ$).

Some of the effects noted here may be masked by higher levels of additive system noise than the $-30$-dB noise-equivalent sigma-naught assumed throughout much of this paper. This was illustrated for the discussion of dynamic range, but the effects of a higher noise level on several other measures can be summarized as follows.

1) Nulls in backscatter versus $\Omega$ curves for HH, HV, and VV will be shallower.
2) Peaks in correlation measures will be lower and nulls shallower.
3) Variations in phase difference measures may be damped.

For repeat-pass interferometry, the dominant source of error may be temporal decorrelation, which would mask any effects due to Faraday rotation. Temporal decorrelation tends to be scatterer dependent, e.g., vegetation canopies tend to decorrelate more than bare oil or rock and may, therefore, be a local phenomenon within a dataset.

Relatively high values of the HV backscatter and/or the HH to HV correlation coefficient may occur naturally within a scene. One mechanism for this to occur is the presence of slopes about the azimuth axis due to topography [21] and [22]. This introduces significant asymmetry into the measurements that may appear at first glance like the effects of Faraday rotation (see Appendix B). The effects of azimuth tilt are separable from those of Faraday rotation, however, since they are:

1) time-invariant;
2) predictable, given a digital elevation model and adequate knowledge of the imaging geometry;
3) local in nature, and will vary considerably across an image with the local terrain slope;

4) can be averaged out if measurements are averaged together over a large enough area;
5) reciprocal (i.e., $Z_{\rm hv} = Z_{\rm vh}$).

Azimuth tilts caused by topography will have no effect on several of the measures considered in this paper, including repeat-pass interferometry (since terrain slopes do not vary), and the phase difference between HV and VH measurements.

Another question we can address with the model results in Section IV is: what is the level of one-way Faraday rotation that will keep distortions in the backscatter signatures from linear polarized SARs below an acceptable level? Table IV shows that the range of backscatter signature distortions expected are within acceptable limits ($\Delta\sigma^{\rm o} < 0.7$ dB, $\Delta\rho < 0.01$, $\Delta\phi < 7^{\circ}$) for $\mathbf{\Omega} \leq 5^{\circ}$. The exception to this (noted above) is the like-to-cross-pol correlation, which is *always* severely distorted by a small Faraday rotation. Some applications (e.g., the recovery of forest biomass from HV backscatter measurements [16]–[18]) may require $\Delta\sigma^{\rm o} < 0.5$ dB, which is only achieved when $\mathbf{\Omega} \leq 3^{\circ}$. The authors hope that researchers in the field will find this work helpful, and look forward to seeing the first unambiguous detection of Faraday rotation in SAR data published.

## Appendix I
## Simple Scattering Models

For slightly rough surfaces (e.g., bare soil), the following model is often used.

### A. Small Perturbation Model

$$\begin{aligned}
&\langle S_{\rm vv} S_{\rm vv}^{*}\rangle = b^2 \langle S_{\rm hh} S_{\rm hh}^{*}\rangle \\
&\langle S_{\rm hh} S_{\rm vv}^{*}\rangle = b\,\langle S_{\rm hh} S_{\rm hh}^{*}\rangle, \qquad b \text{ real},\ b>1 \\
&\langle S_{\rm hv} S_{\rm hv}^{*}\rangle = 0 \\
&\langle S_{\rm hh} S_{\rm hv}^{*}\rangle = \langle S_{\rm hv} S_{\rm vv}^{*}\rangle = 0.
\end{aligned} \tag{A1}$$

The upland forest backscatter is typical of scattering from rotationally symmetric scatterers [19], which have the following general properties.

### B. Rotational Symmetry

$$\begin{aligned}
&\langle S_{\rm hh} S_{\rm hh}^{*}\rangle = \langle S_{\rm vv} S_{\rm vv}^{*}\rangle \\
&\langle S_{\rm hh} S_{\rm vv}^{*}\rangle = \varepsilon \langle S_{\rm hh} S_{\rm hh}^{*}\rangle, \qquad \varepsilon \text{ real} \\
&\langle S_{\rm hv} S_{\rm hv}^{*}\rangle = (1-2\varepsilon)\langle S_{\rm hh} S_{\rm hh}^{*}\rangle \\
&\langle S_{\rm hh} S_{\rm hv}^{*}\rangle = \langle S_{\rm hv} S_{\rm vv}^{*}\rangle = 0.
\end{aligned} \tag{A2}$$

For the forest types with significant double-bounce scatter (i.e., the plantation, swamp forest and conifers), the following model has been used for the double-bounce contribution.

### C. Double-Bounce

$$\begin{aligned}
&\langle S_{\rm vv} S_{\rm vv}^{*}\rangle = |\alpha|^2 \langle S_{\rm hh} S_{\rm hh}^{*}\rangle \\
&\langle S_{\rm hh} S_{\rm vv}^{*}\rangle = \alpha \langle S_{\rm hh} S_{\rm hh}^{*}\rangle, \qquad \alpha \text{ complex} \\
&\langle S_{\rm hv} S_{\rm hv}^{*}\rangle = 0 \\
&[\text{Typically } |\alpha| < 1, \arg(\alpha) \approx \pm\pi].
\end{aligned} \tag{A3}$$

Since canopy scatter and the ground-trunk term are usually present together in the same return, double-bounce and rotationally symmetric (i.e., canopy) scattering need to be combined in some proportion $f_{\rm d} : f_{\rm v}$, as in [20], to give the following.

### D. Rotational Symmetry+Double-Bounce

$$\begin{aligned}
&\langle S_{\rm hh} S_{\rm hh}^{*}\rangle = f_{\rm v} + f_{\rm d} \\
&\langle S_{\rm vv} S_{\rm vv}^{*}\rangle = f_{\rm v} + |\alpha|^2 f_{\rm d} \\
&\langle S_{\rm hh} S_{\rm vv}^{*}\rangle = \varepsilon\, f_{\rm v} + \alpha\, f_{\rm d} \\
&\langle S_{\rm hv} S_{\rm hv}^{*}\rangle = (1-2\varepsilon)\, f_{\rm v} \\
&\langle S_{\rm hh} S_{\rm hv}^{*}\rangle = \langle S_{\rm hv} S_{\rm vv}^{*}\rangle = 0.
\end{aligned} \tag{A4}$$

For $f_{\rm d} \approx f_{\rm v}$, the expected behavior of the combined scattering represented by (A4) has the following properties:

$$\begin{aligned}
\langle S_{\rm hh} S_{\rm hh}^{*}\rangle &\geq \langle S_{\rm vv} S_{\rm vv}^{*}\rangle \\
\rho_{\rm hhvv} &< \varepsilon \\
\text{Re}\,\langle S_{\rm hh} S_{\rm vv}^{*}\rangle &< 0.
\end{aligned} \tag{A5}$$

Note that the general behavior seen in Fig. 1 can be reproduced by inserting the modeled polarization signatures in (A1), (A2) and (A5) into (7). Thus, for slightly rough surfaces, there is a zero point in the predicted "HH" measurement for $\mathbf{\Omega} = 45^{\circ}$, and at $\mathbf{\Omega} = 90^{\circ}$, the "HH" measurement is equal to the VV backscatter value, which is larger than the HH backscatter value. For rotationally symmetric scatterers, the predicted "HH" measurement for $\mathbf{\Omega} = 45^{\circ}$ is the same as the HV backscatter value, and again at $\mathbf{\Omega} = 90^{\circ}$, the "HH" measurement is equal to the VV backscatter value (though both HH and VV values are the same in this case). For mixed rotationally symmetric and double-bounce scatterers, the predicted "HH" measurement for $\mathbf{\Omega} = 45^{\circ}$ is significantly greater than the HV backscatter value, and again at $\mathbf{\Omega} = 90^{\circ}$, the "HH" measurement is equal to the VV backscatter value, which is typically less than or equal to the HH backscatter value.

## Appendix II
## Effects of Azimuth Slopes

After [21] and [22], one can introduce the effects of slopes in the azimuth direction into the measured scattering matrix

$$\begin{pmatrix} Z_{\rm hh} & Z_{\rm vh} \\ Z_{\rm hv} & Z_{\rm vv} \end{pmatrix} = \begin{pmatrix} \cos\theta & -\sin\theta \\ \sin\theta & \cos\theta \end{pmatrix} \cdot \begin{pmatrix} S_{\rm hh} & S_{\rm vh} \\ S_{\rm hv} & S_{\rm vv} \end{pmatrix} \begin{pmatrix} \cos\theta & \sin\theta \\ -\sin\theta & \cos\theta \end{pmatrix} \tag{B1}$$

which becomes

$$Z_{\rm hh} = S_{\rm hh}\cos^2\theta - S_{\rm hv}\sin 2\theta + S_{\rm vv}\sin^2\theta \tag{B2a}$$
$$Z_{\rm vh} = S_{\rm hv}\cos 2\theta + (S_{\rm hh} - S_{\rm vv})\sin\theta\cos\theta \tag{B2b}$$
$$Z_{\rm hv} = S_{\rm hv}\cos 2\theta + (S_{\rm hh} - S_{\rm vv})\sin\theta\cos\theta \tag{B2c}$$
$$Z_{\rm vv} = S_{\rm vv}\cos^2\theta - S_{\rm hv}\sin 2\theta + S_{\rm hh}\sin^2\theta \tag{B2d}$$

assuming reciprocal scattering ($S_{\rm hv} = S_{\rm vh}$).

The expressions given in (B2) contrast with the corresponding expressions for Faraday rotation in (6). The most significant difference is that the cross-pol measurements are still reciprocal in the presence of azimuth slopes (i.e., $Z_{\rm hv} = Z_{\rm vh}$), which is not the case for Faraday rotation.

To determine the effects of azimuth slopes on scattering measurements cross products between the terms in (B2) were formed, and the effects of azimuth tilt angles from 0° to 40° were assessed. The scattering data used was again taken from Table II. Results for $\theta > 0$ were compared with results for $\theta = 0$ and the relative changes are recorded in Table V. The results in Table V confirm those presented in [21] in that azimuth slopes have significant effects on the measurements, particularly on the HV backscatter and the HH to HV correlation term.

## ACKNOWLEDGMENT

The authors would like to thank S. Hensley for some helpful discussions on this topic and the anonymous reviewers for their helpful suggestions to improve the paper. The work described in this paper was carried out by the Jet Propulsion Laboratory, California Institute of Technology, under contract with the National Aeronautics and Space Administration.

## REFERENCES

[1] A. R. Thompson, J. M. Moran, and G. W. Swenson, *Interferometry and Synthesis in Radio Astronomy*. New York: Wiley, 1986.
[2] J. V. Evans and T. Hagfors, *Radar Astronomy*. New York: McGraw-Hill, 1968.
[3] S. H. Bickel and R. H. T. Bates, "Effects of magneto-ionic propagation on the polarization scattering matrix," *Proc. IRE*, vol. 53, pp. 1089–1091, 1965.
[4] W. B. Gail, "A simplified calibration technique for polarimetric radars," in *Proc. IGARSS*, vol. II, Tokyo, Japan, 1993, pp. 377–379.
[5] ——, "Effect of Faraday rotation on polarimetric SAR," *IEEE Trans. Aerosp. Electron. Syst.*, vol. 34, Jan. 1998.
[6] P. Rosen, "Study of Faraday rotation effects on P-band polarimetric spaceborne SAR," JPL, Pasadena, CA, JPL Interoffice Memo. 3343-92-72, 1992.
[7] B. G. Kutuza, A. A. Kalinkevitch, A. I. Ephimov, E. A. Vostrov, and A. B. Dzenkevitch, "Application of SAR operating at P-band for space experiments," in *Proc. EUSAR "96, Eur. Conf. Synthetic Aperture Radar*, Konigswinter, Germany, 1996, pp. 309–313.
[8] T. S. Chu and H. F. Lenzing, "Ionosphere-induced cross polarization of circularly polarized UHF propagation," *IEEE Trans. Antennas Propagat.*, vol. 39, pp. 1644–1647, Nov. 1991.
[9] S. Quegan and J. Lamont, "Ionospheric and tropospheric effects on synthetic aperture radar performance," *Int. J. Remote Sens.*, vol. 7, no. 4, pp. 525–539, 1986.
[10] A. Ishimaru, Y. Kuga, and J. Liu, "Study of ionospheric/tropospheric effects on SAR operation for the JPL/NASA Advanced Radar Technology Program," JPL, Pasadena, CA, Dec. 1997.
[11] E. Rignot, "Effect of Faraday rotation on L-band interferometric and polarimetric synthetic-aperture radar data," *IEEE Trans. Geosci. Remote Sensing*, vol. 38, pp. 383–390, Jan. 2000.
[12] P. Wright, S. Quegan, N. Wheadon, and D. Hall, "Faraday rotation effects on L-band spaceborne SAR data," *IEEE Trans. Geosci. Remote Sensing*, vol. 41, pp. 2735–2744, Dec. 2003.
[13] A. Freeman, "Calibration of linearly polarized polarimetric SAR data subject to Faraday rotation," *IEEE Trans. Geosci. Remote Sensing*, vol. 42, Aug. 2004.
[14] Y. Kuga, private communication, 1999.
[15] A. Freeman, "SAR calibration: An overview," *IEEE Trans. Geosci. Remote Sensing*, vol. 30, pp. 1107–1121, Nov. 1992.
[16] E. J. Rignot, R. Zimmermann, and J. J. van Zyl, "Spaceborne applications of P-band imaging radars for measuring forest biomass," *IEEE Trans. Geosci. Remote Sensing*, vol. 33, pp. 1162–1169, Sept. 1995.
[17] T. Le Toan, A. Beaudoin, J. Riom, and D. Guyon, "Relating forest biomass to SAR data," *IEEE Trans. Geosci. Remote Sensing*, vol. 30, pp. 403–411, Mar. 1992.
[18] M. C. Dobson, F. T. Ulaby, T. LeToan, A. Beaudoin, E. S. Kasischke, and Christiansen, "Dependence of radar backscatter on conifer forest biomass," *IEEE Trans. Geosci. Remote Sensing*, vol. 30, pp. 412–415, Mar. 1992.
[19] S. V. Nghiem, S. H. Yueh, R. Kwok, and F. K. Li, "Symmetry properties in polarimetric remote sensing," *Radio Sci.*, vol. 27, no. 5, pp. 693–711, Sept.-Oct. 1992.
[20] A. Freeman and S. Durden, "A three-component scattering model for polarimetric SAR data," *IEEE Trans. Geosci. Remote Sensing*, pp. 963–973, May 1997.
[21] J. S. Lee, D. L. Schuler, and T. L. Ainsworth, "Polarimetric SAR data compensation for terrain azimuth slope variation," *IEEE Trans. Geosci. Remote Sensing*, vol. 38, pp. 2153–2163, Sept. 2000.
[22] D. L. Schuler, J. S. Lee, and G. De Grandi, "Measurement of topography using polarimetric SAR images," *IEEE Trans. Geosci. Remote Sensing*, pp. 1266–1277, Sept. 1996.
[23] O. K. Garriott, F. L. Smith, and P. C. Yuen, "Observations of ionospheric electron content using a geostationary satellite," *Planet Space Sci.*, vol. 13, pp. 829–838, 1965.

**Anthony Freeman** (M'83–SM'94–F'00) received the B.Sc. (honors) degree in mathematics in 1979 and the Ph.D. degree in astrophysics in 1982, both from the University of Manchester Institute of Science and Technology, Manchester, U.K.

He is currently the Earth Science Program Manager at the Jet Propulsion Laboratory (JPL), Pasadena, CA. Prior to this, he was Section Manager of the Mission and Systems Architecture Section at JPL, responsible for all advanced mission studies at JPL, and prior to that was Instrument Manager for the LightSAR Radar Program. His research interests include correction of Faraday rotation, detection of subsurface features on Mars, and the design of P-Band spaceborne SARs. He is the holder of two patents.

Dr. Freeman was awarded the NASA Exceptional Service Medal for calibration of SIR-C mission data and holds numerous NASA new-technology awards.

**Sasan S. Saatchi** (S'85–M'88) received the B.S. and M.S. degrees in electrical engineering from the University of Illinois, Chicago, in 1981 and 1983 respectively, and the Ph.D. degree from The George Washington University, Washington, DC, in 1988, with the concentration in electrophysics and modeling of wave propagation in natural media.

From 1989 to 1991, he was a Postdoctoral Fellow at the National Research Council and worked at the Laboratory for Terrestrial Physics, NASA Goddard Space Flight Center on the hydrological application of active and passive microwave remote sensing. Since April 1991, he has been with the Radar Science and Engineering Section, Jet Propulsion Laboratory, California Institute of Technology, Pasadena, where as a Scientist, he is involved in developing microwave scattering and emission models for soil and vegetated surfaces and retrieval algorithms for estimating biophysical parameters from spaceborne remote sensing instruments. He has been a Principal or Co-Investigator in several interdisciplinary international projects such as FIFE, EFEDA, Magellan, Mac-Hydro, Hapex-Sahel, BOREAS, LCLUC, and LBA. His current research activities include biomass and soil surface moisture estimation in different ecosystems, land use and land cover change, forest regeneration monitoring over tropical rain forests, and ecological modeling of species range distribution and biodiversity using remote sensing His research interests also include wave propagation in disordered/random media and EM scattering theory. He has been involved in developing and teaching courses in the use of remote sensing for environmental problems.